Journal of Power Sources 223 (2013) 9–17

Contents lists available at SciVerse ScienceDirect

Journal of Power Sources

journal homepage: www.elsevier.com/locate/jpowsour

Performance evaluation of a direct-biogas solid oxide fuel cell-micro gas turbine (SOFC-MGT) hybrid combined heat and power (CHP) system

Suranat Wongchanapai*, Hiroshi Iwai, Motohiro Saito, Hideo Yoshida

Department of Aeronautics and Astronautics, Kyoto University, Yoshida Honmachi, Sakyo-ku, Kyoto 606-8501, Japan

HIGHLIGHTS

- We evaluate a combination of direct-biogas SOFC with MGT CHP system.
- We examine effects of reforming agent, U_f, TIT, compression ratio on system performance.
- The results show the optimal operating parameters on SOFC and system performance.

ARTICLE INFO

Article history:
Received 29 August 2012
Accepted 13 September 2012
Available online 20 September 2012

Keywords:
Solid oxide fuel cell
Biogas
Direct internal reforming
CHP system
Exergy analysis

ABSTRACT

The combination of a direct-biogas solid oxide fuel cell (SOFC) with a micro gas turbine (MGT) system offers great potential as a green decentralized combined heat and power (CHP) system. To evaluate the potential use of biogas as the main source of energy for a direct-biogas SOFC-MGT hybrid CHP system, a sensitivity analysis was conducted under diverse operating conditions to investigate the influence of key operating parameters of the hybrid CHP system with the consideration of operational constraints. The key parameters in this study were SOFC reforming agent, SOFC fuel utilization factor (U_f), turbine inlet temperature (TIT), and compression ratio. The influence of variation in operating parameters on plant performance was evaluated for the overall system and SOFC efficiencies as well as the heat-to-power ratio (TER), the power ratio of MGT to SOFC (P_{MGT}/P_{SOFC}), and the size of the SOFC stack. As a reforming agent for direct-biogas SOFC, steam is more preferable than a traditional air–steam mixture in terms of material limitations and SOFC efficiencies; however, an air–steam mixture with a small amount of air boosts the useful heat output and electricity generated by an MGT without significantly affecting overall system efficiency. The increase in U_f improves the electrical power output produced by the SOFC stack, but also requires more fuel to be fed to the burner, resulting in an increase in useful heat energy. Increasing the compression ratio improves the system electrical efficiency but lowers useful heat generation; nevertheless, increasing TIT decreases the system electrical efficiency but improves the efficiency of the CHP system. To achieve the optimum operating conditions of the hybrid CHP system, the operating parameters should be determined based on the desired energy outcomes.

1. Introduction

Biogas typically refers to a gas produced by the biological breakdown of organic matter in the absence of oxygen. Organic waste such as sludge from municipal wastewater treatment plants, kitchen refuse from households and restaurants, and organic waste from the food-processing industry can be converted into a gaseous fuel called biogas (a mixture of methane, carbon dioxide, and other minor gases). Biogas is a readily available but underexploited energy source, because its high levels of carbon dioxide hinder its use in conventional power-generation systems, resulting in relatively low electrical conversion efficiency. Solid oxide fuel cells (SOFCs) are a promising solution to this problem, owing to their tolerance of fuel contaminants and flexibility of operation even with diluted fuel mixtures.

Direct feeding of biogas to SOFCs has been proven to be feasible for different SOFC configurations and materials by several experimental studies [1–6]. However, during the operation of a direct-biogas SOFC, carbon tends to form, which gradually deactivates the anode catalysts of the system. Shiratori et al. [6] performed an experimental study of anode-supported button-cell SOFCs fuelled by biogas with an internal reforming mode of 800 °C. That study

* Corresponding author. Tel./fax: +81 75 753 5203.
E-mail address: wongchanapai.suranat.72u@st.kyoto-u.ac.jp (S. Wongchanapai).

0378-7753/$ – see front matter © 2012 Elsevier B.V. All rights reserved.
http://dx.doi.org/10.1016/j.jpowsour.2012.09.037

Nomenclature

E_{CH4}	activation energy of the methane reforming reaction
ex	specific exergy flow, kJ kg^{-1}
Ex	exergy flow rate, kW
F	faraday constant, 96,487 C mol^{-1}
HRSG	heat recovery steam generator
HX	heat exchanger
K	equilibrium constants
LHV	lower heating value, kJ kmol^{-1}
M_i	molecular weight of species i, kg mol^{-1}
m	mass flow rate, kg s^{-1}
n_e	number of electrons participating in the electrochemical reaction
n_i	mole flow rate of species i, kmol s^{-1}
P	electrical power, kW
P	total pressure, kPa
p_i	partial pressure of species i, kPa
Q	heat transfer rate, kW
R	universal gas constant, 8.31434 J mol^{-1} K^{-1}
r	reaction rate, kmol s^{-1}
T	temperature, K
TER	heat-to-power ratio
TIT	turbine inlet temperature, K
U_f	fuel utilization factor
V	voltage, V
x_i	mole fraction of species i

Greek letters

ΔG^0	change of standard Gibbs free energy, kJ mol^{-1}
ΔH	enthalpy change, kJ mol^{-1}
η	efficiency
ψ	rational efficiency

Subscripts

0	properties of the environment
act	activation
air	air, air channel
ch	chemical
CHP	combined heat and power overall system
conc	concentration
ele	electrical
FOX	methane full oxidation
fuel	gas mixture at the fuel channel, fuel channel
in	inlet value
inv	inverter
MGT	micro gas turbine
OC	open-circuit
ohm	ohmic
out	outlet value
PEN	positive-electrolyte-negative structure
ph	physical
shift	shift reaction
react	anode reaction
SOFC	solid oxide fuel cell stack
SR	steam reforming
sys	overall system

revealed that the use of air in addition to actual biogas reduces the risk of carbon formation and leads to more stable operation without deteriorating cell voltage due to the lowering of anodic overvoltage.

In parallel with experimental studies, system models have attracted tremendous interest in the past decade as tools for providing theoretical guidance for SOFC-based systems. Yi et al. [7] evaluated integrated SOFC reformer systems and found that system efficiency drops insignificantly by around 1.1% when biogas is used instead of natural gas. Piroonlerkgul et al. [8] investigated the performance of biogas-fed SOFC systems utilizing different reforming agents (steam, air, and combined air/steam) through thermodynamic analysis to determine the most suitable fuel processor. Steam is considered the most suitable reforming agent, as steam-fed SOFCs provide a much higher power density than air-fed ones, although their electrical efficiencies are slightly lower. While adding steam to an air-fed SOFC in the case of a co-fed SOFC can improve power density, it may lower electrical efficiency compared to an air-fed SOFC. Farhad et al. [9,10] performed a sensitivity analysis of three different biogas-reforming processors in SOFC micro-combined heat and power (CHP) systems using a computer model. They considered anode exit gas recirculation, steam reforming, and partial oxidation. In three-dimensional computational fluid dynamics (CFD) simulations preformed by Vakouftsi et al. [11], mass, heat, and momentum transfer equations were combined with chemical and electrochemical phenomena within the inlet region of a planar SOFC unit-cell configuration directly fed with biogas/steam mixtures. When steam was added to biogas, carbon deposition was prevented but the electrical efficiency of the system decreased owing to an increase in voltage losses.

Along with the development of SOFC technology, efforts have been made in the past decade to integrate gas turbines (GTs) with SOFCs to keep pace with rising demand for highly efficient energy production while also minimizing environmental impact. SOFC-GT plants with outputs of tens to hundreds of electrical kilowatts (kW_e) have been demonstrated experimentally [12–17], making conceptual SOFC-GT hybrid systems feasible. Because biogas is increasingly being regarded as a potential renewable energy source for distributed power generation, biogas-fed SOFC-GT systems appear to be one of the most promising alternatives for distributed power generation. Moreover, extending this hybrid system to CHP generation provides heat recovery from exhaust, resulting in high overall efficiency.

In this study, a sensitivity analysis was performed to evaluate the influence of the key operating parameters of a direct-biogas SOFC-micro gas turbine (MGT) hybrid CHP system with an electrical power output of 200 kW_e. Energy and exergy analyses were used to determine the causes of exergy losses and identify areas in need of improvement while adhering to material thermal constraints. Attention was paid to the influence of air–steam mixtures as reforming agents on the direct internally reformed SOFC stack as well as on the SOFC-MGT hybrid CHP plant. The other key operating parameters considered in this study were fuel utilization factor (U_f), turbine inlet temperature (TIT), and compression ratio. The influence of variation in operating parameters on plant performance was evaluated for the overall system and SOFC efficiencies as well as the heat-to-power ratio (TER) and the power ratio of MGT to SOFC (P_{MGT}/P_{SOFC}). Because of the fact that the SOFC stack is the most expensive part in the initial investment cost, the number of cells required in the SOFC stack was also taken into consideration.

2. System configuration and description

A schematic of the direct-biogas SOFC-MGT hybrid CHP system used in this study is shown in Fig. 1. The direct internal-reforming

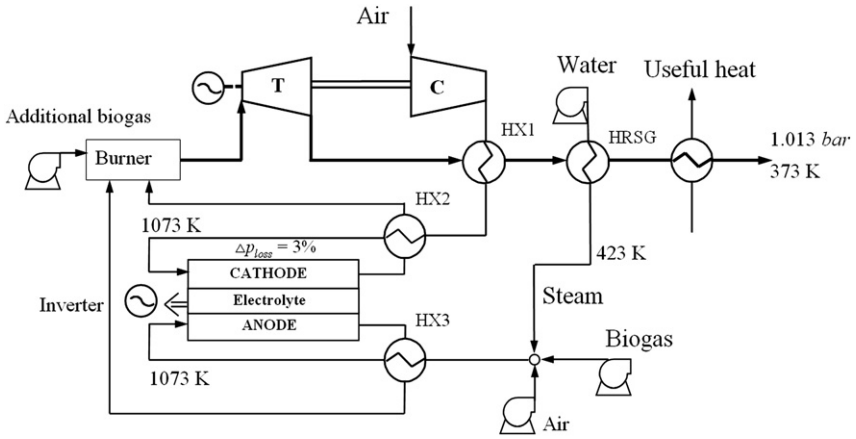

Fig. 1. Schematic flow diagram of the direct-biogas SOFC-MGT hybrid CHP system.

planar SOFC is capable of internal reformation of methane into hydrogen via dry reformation, partial oxidation, and steam reformation reactions. The other peripheral components include an MGT, three gas-to-gas heat exchangers (HX1, HX2, and HX3), a heat recovery steam generator (HRSG), a burner, a water pump, fuel pump, and air pump. The operational parameters for the MGT and other peripheral components are described later.

In the integrated system, because the SOFC does not operate at 100% fuel utilization, a burner is needed to combust excess and additional fuel to elevate the TIT to a specified range for optimum system performance. Then, the products of the burner expand in the turbine and the exhausted gas is further utilized by HX1 and HRSG. Before the flue gas is released into the environment at atmospheric pressure, it is cooled to 373 K, producing useful heat. The SOFC air and fuel streams are preheated by the cathode and anode off-gases in HX2 and HX3 and are heated up to 1073 K. An inverter is also used in the system to convert the DC power output of the SOFC stack into AC power output. To prevent carbon deposition in the SOFC, biogas is mixed with air and/or steam before it enters the cell. An HRSG is integrated at the MGT exhaust outlet, supplying a predetermined amount of steam while a small amount of air from an air pump is mixed with the fuel. For all of the HXs and the HRSG, a 2% heat loss is assumed. Possible variation in pressure drop across each component is assumed to be 2%, except in the SOFC, where it is assumed to be 3%.

3. System modeling

The integrated system components (e.g., SOFC, MGT, HXs, burner, HRSG, and air and fuel pumps) were thermodynamically modeled under steady-state conditions. Mass and energy balances were applied for each component using lumped models, which consider each component as a control volume, with the exception of a one-dimensional SOFC model based on previous work [18]. The following assumptions were made: (i) all system components operate under steady-state conditions; (ii) all gas mixtures behave as ideal gases; (iii) the biogas is clean and chemically stable; (iv) heat loss from the SOFC is negligible and those from HXs and the HRSG are 2% of the heat transferred; and (v) chemical reactions are in equilibrium.

3.1. Direct-biogas SOFC modeling

The direct internal-reforming SOFC model developed in a recent work by the authors [18] was modified to include dry-reforming and partial-oxidation reactions owing to the presence of CO_2 and O_2 in the anode. The model is capable of capturing the distribution of local temperatures, species concentrations, current density, and polarization losses in the streamwise direction. The electrochemical reaction is considered to be attributable to hydrogen only; the electrochemical fuel value of CO is readily exchanged for hydrogen by the rapid shift reaction, assuming chemical equilibrium [19].

Dry reforming is perhaps the most interesting option for the conversion of biogas because the major constituents of biogas are carbon dioxide and methane. However, the dry-reforming reaction is prone to carbon deposition, which in turn can cause rapid catalyst deactivation [20,21]. Because steam and dry-reforming reactions are intensively endothermic, it is necessary to supply high-temperature inlet streams to the SOFC stack; however, this reduces the overall efficiency of the system. This problem can be overcome by applying an exothermic partial-oxidation reaction that utilizes air as the reforming agent. However, the nature of the partial oxidation of methane is a matter of debate when fuel gas and oxidant are mixed. Hibino [22,23] and Buergler [24] have suggested that in the case of fuel in a nickel anode channel, partial oxidation of methane takes place via a two-step mechanism. First, full oxidation of methane takes place, producing CO_2 and H_2O; then, synthesis gas is produced via steam reformation of unreacted methane while the water-gas shift reaction is at equilibrium.

Mass balances are formulated for each species on the basis of the relationship between the local current and changes in concentrations. The following equations summarize the reactions considered in the fuel cell stack.

Full oxidation of CH_4 in the oxygen-rich zone yielding CO_2 and H_2O:

$$\text{Full oxidation of methane}: \quad CH_4 + 2O_2 \rightarrow CO_2 + 2H_2O \qquad (1)$$

Syngas can be generated by reforming reactions of unused methane reacting with H_2O or CO_2:

$$\text{Steam reforming}: \quad CH_4 + H_2O \rightarrow CO + 3H_2 \qquad (2)$$

$$\text{Dry reforming}: \quad CH_4 + CO_2 \rightarrow 2CO + 2H_2 \qquad (3)$$

The water–gas shift reaction converts CO into H_2, which is more easily electrochemically oxidized than CO:

$$\text{Water} - \text{gas shift reaction}: \quad CO + H_2O \leftrightarrow CO_2 + H_2 \tag{4}$$

$$\text{Overall cell reaction}: \quad H_2 + \frac{1}{2}O_2 \rightarrow H_2O \tag{5}$$

The respective reaction rate equation for total oxidation [25] described in (Eq. (1)) on supported Ni catalysts is given as follows:

$$r_{FOX} = \frac{k_a \cdot p_{CH_4} \cdot p_{O_2}}{\left(1 + K^{OX}_{CH_4} \cdot p_{CH_4} + K^{OX}_{O_2} \cdot p_{O_2}\right)^2} + \frac{k_b \cdot p_{CH_4} \cdot p_{O_2}}{\left(1 + K^{OX}_{CH_4} \cdot p_{CH_4} + K^{OX}_{O_2} \cdot p_{O_2}\right)} \tag{6}$$

where p_i is the partial pressure of component i in the gas mixture.

The Arrhenius reaction rate for component i in combustion reaction k_i is expressed as

$$k_i = A(k_k)\exp\left(\frac{E_k}{R \cdot T}\right) \tag{7}$$

The adsorption constant for component i in combustion reaction K_i^{OX} is expressed as

$$K_i^{OX} = A(K_i)\exp\left(\frac{\Delta H_{k,i}}{R \cdot T}\right) \tag{8}$$

The reaction rate of the steam-reforming reaction is expressed as

$$r_{SR} = k_{CH_4}\left(1 - \frac{p_{CO} \cdot p^2_{H_2}}{p_{CH_4} \cdot p_{H_2O} \cdot K_{eq,SR}}\right) p_{CH_4} \exp\left(\frac{-E_{CH_4}}{R \cdot T}\right) \tag{9}$$

where E_{CH4} (=82 kJ mol^{-1}) is the activation energy of the reaction and k_{CH4} (=4274 mol m^{-2} bar^{-1} s^{-1}) is the pre-exponential factor (Table 1).

The dry-reforming reaction (Eq. (3)) is not explicitly included but is implicitly considered through the water–gas shift reaction (Eq. (4)). As mentioned above, the water–gas shift reaction was always assumed to be at equilibrium in this study. The equilibrium constant for this reaction and the steam-reforming reaction can be described as follows [26]:

$$K_{p,shift} = \exp\left(-0.2935Z^3 + 0.6351Z^2 + 4.1788Z + 0.3619\right) \tag{10}$$

$$K_{eq,SR} = 1.0267 \times 10^{10}\exp\left(-0.2513Z^4 + 0.3665Z^3 + 0.5810Z^2 - 27.134Z + 3.2770\right) \tag{11}$$

where $Z = (1000/T) - 1$.

The open-circuit voltage (V_{OC}) is described by the Nernst equation as a function of operating temperature (T) and partial pressure (p):

$$V_{OC} = \frac{\Delta G^0}{2F} + \frac{R \cdot T}{2F} \cdot \ln\left(\frac{p_{H_2} \cdot p^{1/2}_{O_2}}{p_{H_2O}}\right) \tag{12}$$

where the Faraday constant (F) = 96,485 A mol^{-1}.

The terminal voltage of the single cell can be obtained as follows:

$$V = V_{OC} - V_{act} - V_{ohm} - V_{conc} \tag{13}$$

The terminal voltage of the cell is lower than the open-circuit voltage when the current is drawn from the cell, owing to three types of overpotential losses: activation (V_{act}), ohmic (V_{ohm}), and concentration (V_{conc}) losses. The evaluations of the losses in the present study are the same as those in our previous report [18] and are not described here. The power output of the SOFC stack is

$$P_{SOFC} = \eta_{inv} \cdot V\left[2F\left(n_{H_2,react} + n_{CO,react} + 4n_{CH_4,react}\right)\right] \tag{14}$$

where η_{inv} is the inverter efficiency.

3.2. System parameters and efficiencies

Because the fuel is not completely consumed by electrochemical reactions in the anode channel, the rate of excess fuel flow is determined by U_f, a key parameter investigated in this study. U_f is defined here as the ratio of fuel consumed by anode reactions to the fuel entering anode channels, and is expressed as

$$U_f = \frac{n_{H_2,react} + n_{CO,react} + 4n_{CH_4,react}}{\left(n_{H_2,SOFC} + n_{CO,SOFC} + 4n_{CH_4,SOFC}\right)_{in}} \tag{15}$$

The TER of the combined plant indicates the ratio of useful thermal energy to electricity generation. It is determined as

$$TER = \frac{Q_{useful}}{P_{SOFC} + P_{MGT}} \tag{16}$$

We defined two types of efficiencies: energetic (or fuel) efficiency and rational efficiency for steady-state processes, as described by Kotas [27].

3.2.1. Energetic efficiency (η)

In any system, energetic efficiency is defined as the ratio of energy in the product output to the energy in the fuel input. It can be applied practically as follows:

The SOFC efficiency can be determined as

$$\eta_{SOFC} = \frac{P_{SOFC}}{\sum_{CH_4,CO,H_2}\left(m_{anode} \cdot LHV\right)_{in}} \times 100\% \tag{17}$$

The system electrical efficiency for a power generation system is defined as

Table 1
Calculation-based parameters for the reaction rate constants in Eq. (7) and the adsorption constants in Eq. (8) (taken from Ref. [25]).

	$A(k_k)$	E_k (kJ mol^{-1})		$A(K_i)$	ΔH_k (kJ mol^{-1})
k_a (kmol kg$_{cat}^{-1}$bar^{-2}h^{-1})	2.92×10^6	86.0	$K^{OX}_{CH_4}$ (bar^{-1})	1.26×10^{-1}	−27.3
k_b (kmol kg$_{cat}^{-1}$bar^{-2}h^{-1})	2.46×10^6	86.0	$K^{OX}_{O_2}$ (bar^{-1})	7.87×10^{-7}	−92.8

$$\eta_{ele,sys} = \frac{P_{SOFC} + P_{MGT}}{\left(m_{biogas} \cdot LHV_{biogas}\right)_{in}} \times 100\% \quad (18)$$

The CHP system efficiency is defined as

$$\eta_{CHP} = \frac{P_{SOFC} + P_{MGT} + Q_{useful}}{\left(m_{biogas} \cdot LHV_{biogas}\right)_{in}} \times 100\% \quad (19)$$

To gain more insight into the system, exergy analysis was used to identify and locate irreversibility. The exergy associated with a material stream is equal to the maximum amount of work obtainable when the stream is brought from its initial state to the dead state. The exergy transfer rate associated with a material stream can be divided into physical and chemical exergy components:

$$Ex = n\left(ex_{ph} + ex_{ch}\right) \quad (20)$$

Physical exergy is the work obtainable by taking the substance through reversible processes from its initial state at temperature T and pressure P to the environmental state. It can be calculated as

$$ex_{ph} = \sum_i x_i[(h - h_0) - T_0(s - s_0)]_i \quad (21)$$

where h is the specific enthalpy, s is the specific entropy, and the properties indicated with the subscript 0 refer to the environmental state.

Chemical exergy is equal to the maximum amount of work obtainable when the substance under consideration is brought from the environmental state, defined by the parameters T_0 and P_0, to the reference state by processes involving heat transfer and exchange of substances only with the environment. The chemical exergy for mixtures can be expressed as

$$ex_{ch} = \sum_i x_i \cdot ex_{0,i} + RT_0 \sum_i x_i \ln(x_i) \quad (22)$$

where $ex_{0,i}$ denotes the standard molar chemical exergy of the i-th species, assuming the reference atmospheric composition given by Kotas [27]. The exergy transfer connected with the heat transfer rate Q at temperature T can be expressed as

$$Ex_Q^T = Q\left(\frac{T - T_0}{T_0}\right) \quad (23)$$

3.2.2. Rational efficiency (ψ)

Rational efficiency is defined by Kotas [27] as the ratio of the desired exergy output to the exergy used or consumed. It provides a realistic indicator of a system's efficiency by applying the exergy of the working fluid at the outlet of a component to the next component.

The SOFC rational efficiency is defined as

$$\psi_{SOFC} = \frac{P_{SOFC}}{\left(Ex_{fuel} + Ex_{air}\right)_{SOFC,in} - \left(Ex_{fuel} + Ex_{air}\right)_{SOFC,out}} \times 100\% \quad (24)$$

The rational efficiency for CHP system is defined as

$$\psi_{CHP} = \frac{P_{SOFC} + P_{MGT} + Ex_Q^T}{Ex_{fuel,sys} - Ex_{exhaust}} \times 100\% \quad (25)$$

Table 2
Operational parameter values for the SOFC simulation.

Parameters	Value
Biogas	CH_4 60%:CO_2 40%
Stack input data	
Fuel utilization factor U_f (−)	0.75
Air utilization factor U_a (−)	0.25
Average current density (A/m^2)	4000
Number of channels per SOFC cell	20
Air inlet temperature to the SOFC $T_{air,in}$ (K)	1073
Fuel inlet temperature to the SOFC $T_{fuel,in}$ (K)	1073
Cell length (mm)	100.0
Width covered by one channel (mm)	5.0
Air channel height (mm)	1.5
Fuel channel height (mm)	0.4
Anode thickness (μm)	500
Cathode thickness (mm)	50
Electrolyte thickness (μm)	10

4. Simulation results

4.1. Computational conditions

Because the SOFC stack is considered the central part of the hybrid system, the simulation results are presented in two parts. First, the performance of the biogas-fed SOFC operated at atmospheric pressure utilizing different reforming agents (steam and combined air/steam) was investigated via thermodynamic analysis to determine the most suitable feed, using the operational parameter values listed in Table 2. SOFC performance under co-flow operation was also analyzed because it generally has a more uniform temperature distribution than other flow configurations [18]. These results are discussed first. The second part presents the sensitivity analysis of the direct-biogas SOFC-MGT hybrid CHP system shown schematically in Fig. 1. To understand the operational scenarios of the hybrid CHP system, an independent parameter analysis of a single component is not enough to assess the whole system, because all components in the system affect one another. The input operational parameter values for the SOFC and the other system components presented in Tables 2 and 3 were used as constants throughout the study, unless indicated otherwise.

The inlet gas compositions are determined by considering the carbon-hydrogen-oxygen (C–H–O) ternary diagrams shown in Fig. 2. In principle, it is feasible to directly feed biogas containing the natural reforming agent, CO_2, into a high-temperature SOFC without an additional reforming agent. However, in regard to the most common form of biogas considered in this work (represented

Table 3
Operational parameter values for system simulation.

Parameters	Value
Total electrical net output power (kW)	200
Steam-to-carbon ratio (−)	2
Compression ratio (−)	8
Turbine inlet temperature TIT (K)	1073
Exhaust gas temperature (K)	373
Pump isentropic efficiency η_{pump} (−)	0.95
Air compressor isentropic efficiency (−)	0.75
Fuel compressor isentropic efficiency (−)	0.75
Turbine isentropic efficiency (−)	0.85
Pump mechanical efficiency (−)	0.98
Air compressor mechanical efficiency (−)	0.98
Fuel compressor mechanical efficiency (−)	0.98
Turbine mechanical efficiency (−)	0.98
Inverter efficiency η_{inv} (−)	0.95

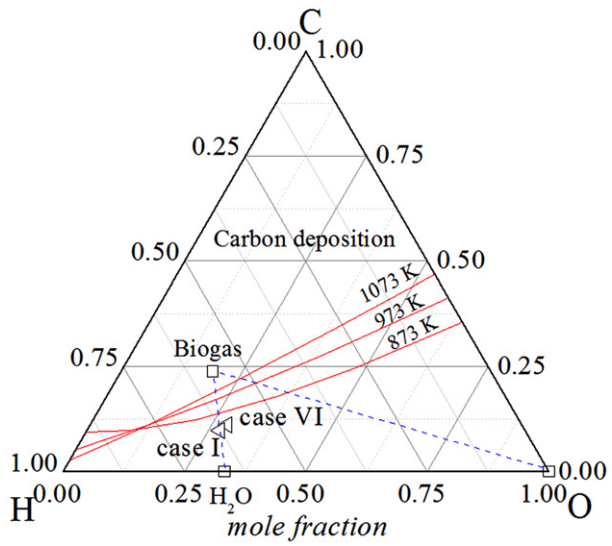

Fig. 2. C–H–O ternary diagram with a carbon deposition boundary at 1073, 973, and 873 K and 1 atm.

by 60% CH_4 and 40% CO_2 in volume), biogas lies above the carbon deposition boundary curves, indicating that solid carbon exists in heterogeneous equilibrium. The location of biogas may be moved below the carbon deposition boundary by adding steam or oxygen. As clearly shown in Fig. 2, an increase in steam or oxygen as a reforming agent for methane in biogas can minimize the risk of carbon deposition. In this study, six different inlet gas compositions were examined. Cases I and VI are shown in Fig. 2; the others (cases II–V) are not shown in the figure but are located somewhere between these two points. Detailed gas compositions are explained in the next section (Fig. 3).

4.2. Direct-biogas SOFC simulation

A strong endothermic reaction due to the presence of steam can lead to local temperature gradients, especially near the entrance of the stack, resulting in mechanical failure due to thermally induced stress. In this study, the maximum allowable temperature gradient and the maximum allowable cell temperature, which are the most important operational constraints for a planar SOFC, were set to 1300 K and 5 K mm^{-1}, respectively, following Stiller et al. [28].

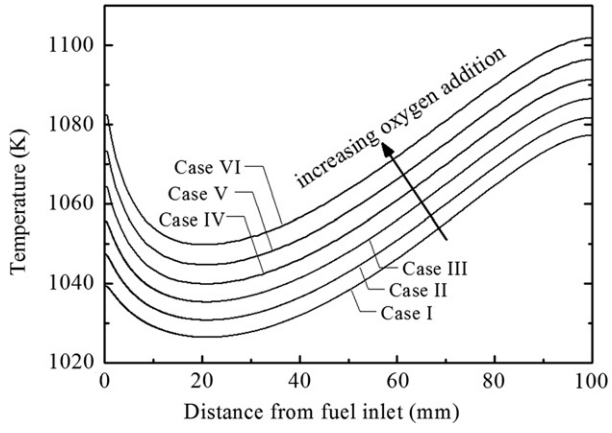

Fig. 3. SOFC cell temperature profiles for different air–steam mixtures as SOFC reforming agents.

Table 4 presents the sensitivity of the system to different ratios of air and steam to fuel for cases I–VI, illustrating how reforming agents may affect SOFC performance. As mentioned in the previous section, anode feed gases were located below the carbon deposition boundary in all cases. As shown in Table 4, an increase in air input into the anode deteriorated the SOFC energetic and rational efficiencies from 50.8% to 47.4% and from 72.3% to 70.0%, respectively, mainly due to partial oxidation. The SOFC cell temperature profiles for the six different ratios of air and steam to fuel are depicted in Fig. 2. The presence of oxygen caused the cell temperature near the channel inlets to rise, and consequently accelerated the strong endothermic reactions that take place during the steam reformation of methane. As the steam-reforming reaction rate increases, the cell temperature drops more rapidly and the cell temperature gradient becomes steeper near the gas inlets. The maximum cell temperatures ($T_{PEN,\ max}$) and the maximum cell temperature gradients $(\partial T_{PEN}/\partial x)_{max}$ corresponding to Fig. 2 are listed in Table 4. According to the table, only cases I–IV led to safe operation of the system under the material constraints. The most favorable operating conditions were in case I, which had the lowest maximum temperature gradient and the highest energetic (η_{SOFC}) and rational efficiencies (ψ_{SOFC}). It should be noted, however, that a high exhaust gas temperature is favorable for hybrid operation. The effects of reforming agents on the hybrid CHP system are discussed later in this report.

4.3. System simulation

A sensitivity analysis was used to quantify the effects of air–steam mixtures as reforming agents, U_f, TIT, and the compression ratio on system performance and the size of the SOFC stack.

4.3.1. Influence of air–steam mixtures as reforming agents

The efficiencies of the direct-biogas SOFC-MGT hybrid CHP system under various air–steam mixtures as reforming agents (anode feed gas compositions of cases I–V in Table 3) are depicted in Fig. 4. As the amount of air input increased, both the SOFC energetic (η_{SOFC}) and the SOFC rational efficiencies (ψ_{SOFC}) decreased, while the exhaust heat from the SOFC increased. This compensated for the drop in electrical power produced by the SOFC stack. These results suggest that air–steam mixtures have only slight effects on system electrical efficiency ($\eta_{ele,syn}$), CHP system efficiency (η_{CHP}), and CHP system rational efficiency (ψ_{CHP}). The effects of air–steam mixtures as reforming agents on the required number of SOFC cells, the output power ratio of MGT to SOFC (P_{MGT}/P_{SOFC}), and the TER of the direct-biogas SOFC in the hybrid CHP system are shown in Fig. 5. At an air:biogas ratio of 0.4, the required number of cells decreased by approximately 4%, whereas P_{MGT}/P_{SOFC} increased from 0.37 to 0.40. As more air was added, TER increased from 0.38 to 0.41 owing to more heat energy in the SOFC off-gases going to the MGT system, leading to a reduction in the fuel fed to the burner. It should be noted that only the anode feed gas composition of case I was used for the rest of the system evaluation.

Table 4
Summary of SOFC performance at atmospheric pressure based on different SOFC reforming agents.

Case	Biogas:steam:air	η_{SOFC} (%)	ψ_{SOFC} (%)	$T_{PEN,\ max}$ (K)	$(\partial T_{PEN}/\partial x)_{max}$(K/mm)
I	1:2.0:0.0	50.8	72.3	1077.1	1.6
II	1:1.9:0.1	50.2	71.9	1081.5	2.4
III	1:1.8:0.2	49.6	71.5	1086.3	3.3
IV	1:1.7:0.3	48.9	71.2	1091.1	4.3
V	1:1.6:0.4	48.0	70.7	1096.2	**5.4**
VI	1:1.5:0.5	47.4	70.0	1101.7	**6.5**

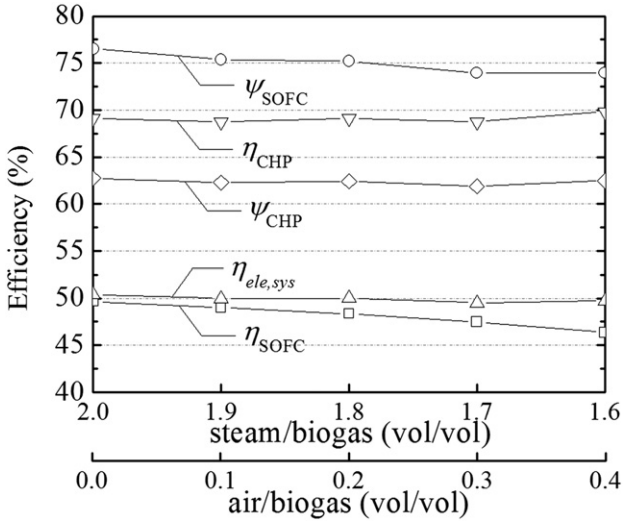

Fig. 4. Influence of air–steam mixtures as reforming agents on SOFC and system efficiencies.

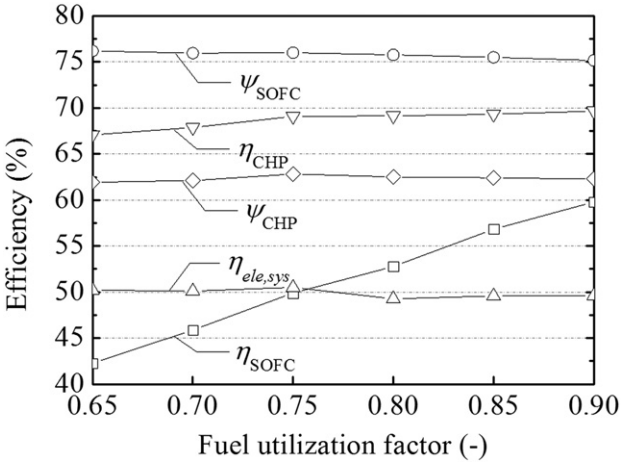

Fig. 6. Influence of the fuel utilization factor on SOFC and system efficiencies.

4.3.2. *Influence of U_f*

The U_f of a commercial SOFC is 75–85% [29]. U_f is an important parameter, which is closely related to the performance of SOFCs and exhaust heat, reflecting the performance of hybrid CHP systems. The proper amounts of exhaust heat and unreacted fuel from the electricity conversion process result in an efficient GT cycle. The influence of U_f on SOFC and system performance is shown in Fig. 6. As U_f increased from 0.65 to 0.90, SOFC energetic efficiency (η_{SOFC}) and CHP system efficiency (η_{CHP}) increased from 42.3% to 59.8% and from 67.1 to 69.7%, respectively. The significant increase of η_{SOFC} is due to the fact that as U_f is enhanced, electrochemical reaction rates increase, thus raising the electrical power output produced by the SOFC stack. However, when considering exergy in the outgoing streams, the SOFC rational efficiency (ψ_{SOFC}) peaked at 76.2% when U_f was 0.65, while CHP system rational efficiency (ψ_{CHP}) was relatively constant around 62%. The influence of U_f on the required number of SOFC cells, P_{MGT}/P_{SOFC}, and TER is presented in Fig. 7. At a U_f of 0.75, the required number of cells was lowest (5277) among all of the cases studied. This is mainly due to compensation between the electrical power produced by the MGT and the SOFC. As U_f changed from 0.65 to 0.90, P_{MGT}/P_{SOFC} dropped from 0.41 to 0.36, owing to a considerable increase in the SOFC efficiency. When U_f increases, it results in less unused fuel in the anode exhaust, and consequently, more additional fuel is needed to maintain the set TIT. At the same time, TER increased from 0.34 to 0.40, because the amount of heat in flue gas increased as the amount of additional fuel fed to the burner increased.

4.3.3. *Influence of compression ratio and TIT*

The compression ratio and TIT are key design parameters of an MGT-SOFC hybrid system, because they considerably affect the heat balance between the MGT and SOFC units. In the present study, the compression ratio and TIT were varied from 2 to 12 and 973 to 1273 K, respectively. In Fig. 8, the effects of compression ratio and TIT on the CHP system efficiency (η_{CHP}) and CHP system rational efficiency (ψ_{CHP}) are plotted. It should be noted that when the compression ratio is set at 12 with an input operational U_f of 0.75, TIT exceeds 973 K. Therefore, no data point for this case is shown in the figure. As can be seen in the figure, at a compression ratio between 2 and 3, the deviation of η_{CHP} was not significant. However, when the ratio was increased from 3 to 12, η_{CHP} decreased linearly. This is because increasing the compression ratio reduces the amount of useful heat available, resulting in a decrease in η_{CHP}. On the other hand, when considering exergy in exhaust gas, ψ_{CHP} increased with an increase in the compression ratio, and the

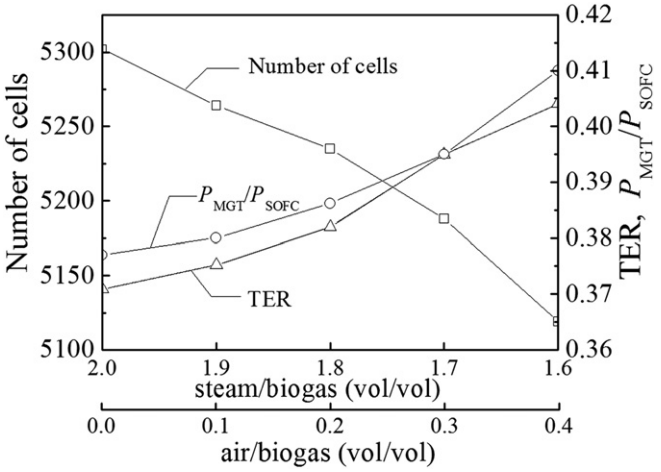

Fig. 5. Influence of air–steam mixtures as reforming agents on P_{MGT}/P_{SOFC}, TER, and the required number of SOFC cells.

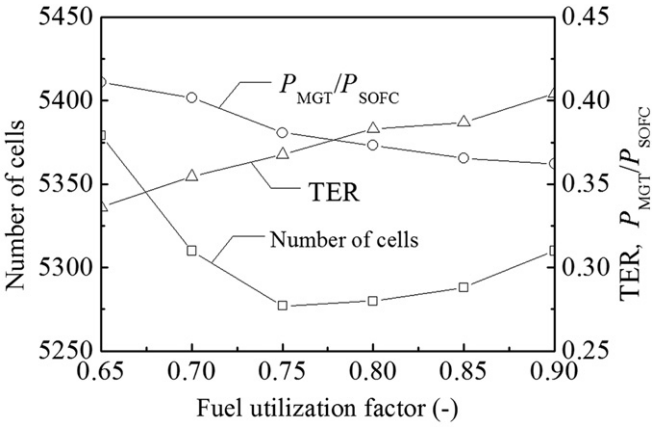

Fig. 7. Influence of the fuel utilization factor on P_{MGT}/P_{SOFC}, TER, and the required number of SOFC cells.

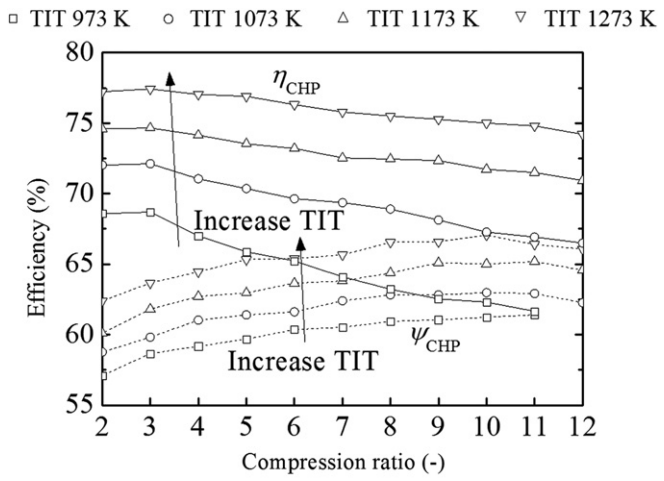

Fig. 8. η_{CHP} and ψ_{CHP} versus compression ratio and TER.

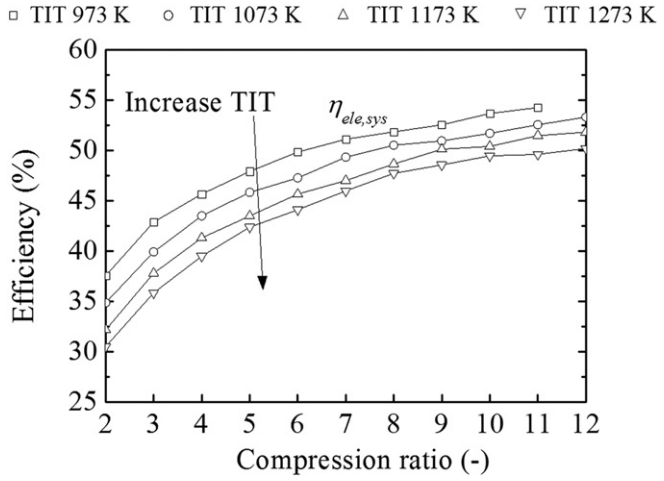

Fig. 9. Influence of compression ratio and TIT on system electrical efficiency.

optimum ψ_{CHP} was achieved at a compression ratio in the range of 9–11. In addition, increasing TIT considerably improved the η_{CHP} and ψ_{CHP} of the system. This is because the production of byproduct heat is significantly boosted with increasing TIT.

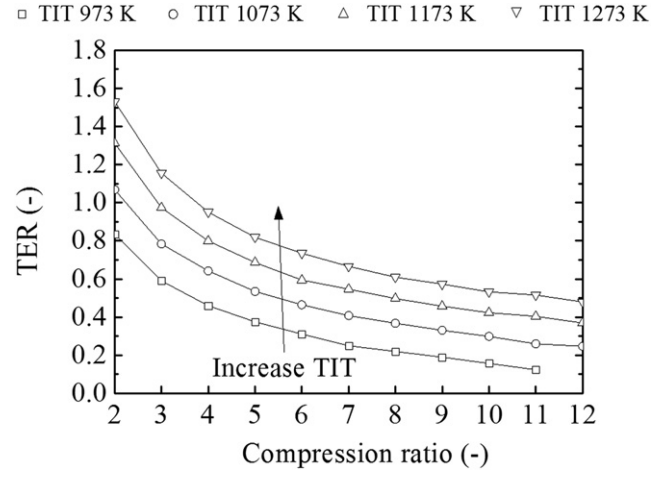

Fig. 10. Influence of compression ratio and TIT on TER.

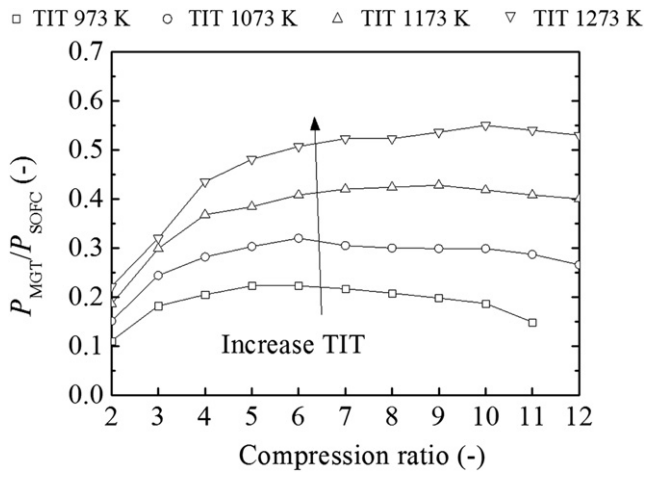

Fig. 11. Influence of compression ratio and TIT on P_{MGT}/P_{SOFC}.

However, as TIT increases, more additional fuel is supplied to the burner, leading to an increase in the system fuel consumption rate. This also results in lower net system electrical efficiency. Indeed, as can be seen in Fig. 9, increasing TIT in the present study had a negative impact on system electrical efficiency ($\eta_{ele,sys}$) due to an increase in fuel feed. In addition, increasing the compression ratio from 2 to 12 enhanced $\eta_{ele,sys}$ by approximately 18% (Fig. 9). The system electrical efficiency increased more rapidly at a low compression ratio. As shown in Fig. 10, the TER increased with an increase in TIT, as more heat that is useful was produced. Nevertheless, the TER decreased with an increase in compression ratio, because the MGT gains efficiency as electricity is generated. Variation in P_{MGT}/P_{SOFC} according to compression ratio and TIT is shown in Fig. 11. The P_{MGT}/P_{SOFC} reached a maximum value at a compression ratio between 5 and 10 when TIT ranged from 973 to 1273 K. The maximum value of P_{MGT}/P_{SOFC} shifts toward a higher compression ratio as TIT increases. As can be seen in Fig. 12, at lower compression ratios, the required number of SOFC cells decreased significantly and reached a minimum value at a compression ratio in the vicinity of 8. In addition, increasing TIT reduced the required number of SOFC cells. This is mainly because the portion of electrical power generated by MGT increases as TIT increases, leading to a reduction in the required number of SOFC cells.

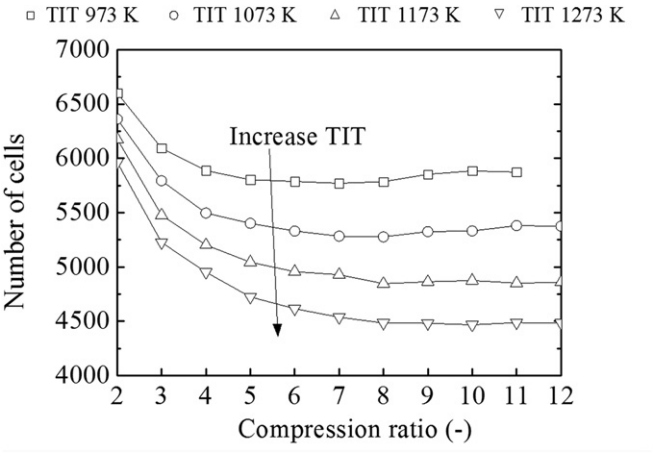

Fig. 12. Influence of compression ratio and TIT on the required number of SOFC cells.

5. Conclusions

Performance evaluations of a direct-biogas SOFC-MGT hybrid CHP system were conducted. It is important to closely monitor the operational performance of SOFCs to minimize SOFC degradation due to thermal constraints and carbon deposition on Ni-based anodes. The main SOFC model used in this study was based on previous work [18], whereas other system components were zero-dimensional component models. Sensitivity analysis was carried out to investigate the influences of the main variables on the system. The main parameters considered were air–steam mixtures as reforming agents, U_f, TIT, and the compression ratio. Based on the results of our simulations, the following conclusions can be made:

- Considering individual direct-biogas SOFC operation, as the average cell operating temperature increases as more air is added to the biogas, carbon deposition is less likely to form in the anode channels. Nevertheless, the presence of oxygen has a negative impact on SOFC performance and also causes temperature stress near the stack inlet due to partial oxidation.
- The addition of a small amount of air to biogas does not have a significant effect on $\eta_{ele,syn}$, η_{CHP}, or ψ_{CHP} of the direct-biogas SOFC in the hybrid CHP system. However, it raises the stack operating temperature and leads to an increase in useful heat output as well as electrical power production by the MGT, which in turn reduces the number of SOFC cells required.
- In the system studied, the electrical power output produced by the SOFC stack was directly proportional to U_f; however, $\eta_{ele,syn}$ was not significantly affected by variation in U_f. The smallest number of cells was achieved at a U_f of 0.75, whereas the TER increases with an increase in U_f.
- Increasing the compression ratio improves $\eta_{ele,sys}$ but reduces TER, whereas increasing TIT has the opposite outcomes. However, increasing the compression ratio and TIT has the same influence on ψ_{CHP}, P_{MGT}/P_{SOFC}, and the required number of SOFC cells.

References

[1] J. Staniforth, K. Kendall, Journal of Power Sources 86 (2000) 401–403.
[2] K. Girona, J. Laurencin, M. Petitjean, J. Fouletier, F. Lefebvre-Joud, ECS Transactions 25 (2) (2009) 1041–1050.
[3] A. Lanzini, P. Leone, International Journal of Hydrogen Energy 35 (2010) 2463–2476.
[4] P. Leone, A. Lanzini, M. Santarelli, M. Cali, F. Sagnelli, A. Boulanger, A. Scaletta, P. Zitella, Journal of Power Sources 195 (2010) 239–248.
[5] Y. Shiratori, T. Oshima, K. Sasaki, International Journal of Hydrogen Energy 33 (2008) 6316–6321.
[6] Y. Shiratori, T. Ijichi, T. Oshima, K. Sasaki, International Journal of Hydrogen Energy 35 (2010) 7905–7912.
[7] Y. Yi, A.D. Rao, J. Brouwer, G.S. Samuelsen, Journal of Power Sources 144 (2005) 67–76.
[8] P. Piroonlerkgul, S. Assabumrungrat, N. Laosiripojana, A.A. Adesina, Chemical Engineering Journal 140 (2008) 341–351.
[9] S. Farhad, F. Hamdullahpur, Y. Yoo, International Journal of Hydrogen Energy 35 (2010) 3758–3768.
[10] S. Farhad, Y. Yoo, F. Hamdullahpur, Journal of Power Sources 195 (2010) 1446–1453.
[11] E. Vakouftsi, G.E. Marnellos, C. Athanasiou, F. Coutelieris, Solid State Ionics 192 (1) (2011) 458–463.
[12] S.E. Veyo, L.A. Shockling, J.T. Dederer, J.E. Gillett, W.L. Lundberg, Journal of Engineering for Gas Turbines and Power 124 (2002) 845–849.
[13] S.E. Veyo, S.D. Vora, K.P. Litzinger, W.L. Lundberg, Status of pressurized SOFC/GAS turbine power system development at Siemens Westinghouse, in: Proceedings of the ASME Turbo Expo, Amsterdam, Netherlands (2002).
[14] K.P. Litzinger, Comparative evaluation of SOFC gas turbine hybrid options, in: Proceedings of the ASME Turbo Expo Conference, Reno, NV, USA (2005).
[15] D.G.D. Agnew, The design and integration of the rolls royce fuel cell systems 1MW SOFC, in: Proceedings of the ASME Turbo Expo Conference, Reno, NV, USA (2005).
[16] M.L. Ferrari, M. Pascenti, R. Bertone, L. Magistri, Journal of Fuel Cell Science and Technology 6 (2009) 031008-1–031008-8.
[17] http://www.mhi.co.jp/en/news/sec1/200608041128.html, May 1, 2008.
[18] S. Wongchanapai, H. Iwai, M. Saito, H. Yoshida, Journal of Power Sources 204 (2012) 14–24.
[19] M.A. Khaleel, Z. Lin, P. Singh, W. Surdoval, D. Collin, Journal of Power Sources 130 (2004) 136–148.
[20] T. Kim, S. Moon, S. Hong, Applied Catalysis A: General 224 (2002) 111–120.
[21] M.W. Li, G.H. Xu, Y.L. Tian, L. Chen, H.F. Fu, Journal of Physical Chemistry A 108 (2004) 1687–1693.
[22] T. Hibino, S. Wang, S. Kakimoto, M. Sano, Electrochemical and Solid-State Letter 2 (1999) 317–319.
[23] T. Hibino, A. Hashimoto, T. Inoue, J. Tokuno, S. Yoshida, M. Sano, Journal of the Electrochemical Society 147 (2000) 2888–2892.
[24] B.E. Buergler, A.N. Grundy, L.J. Gauckler, Journal of the Electrochemical Society 153 (2006) A1378–A1385.
[25] C.R.H. de Smet, M.H.J.M. de Croon, R.J. Berger, G.B. Marin, J.C. Schouten, Chemical Engineering Science 56 (16) (2001) 4849–4861.
[26] M.V. Twigg, Catalyst Handbook, Wolfe Pub. Ltd, London, 1989.
[27] T.J. Kotas, The Exergy Method of Thermal Plant Analysis, second ed., (1995). USA.
[28] C. Stiller, B. Thorud, S. Seljebø, Ø. Mathisen, H. Karoliussen, O. Bolland, Journal of Power Sources 141 (2005) 227–240.
[29] R.J. Braun, Optimal design and operation of solid oxide fuel cell systems for small-scale stationary applications, Ph.D thesis, University of Wisconsin-Madison, USA (2002).